Chapter 11

Use of Wavelet Techniques in the Study of Seawater Flux Dynamics in Coastal Lakes

Edwin Muchebve, Yoshiyuki Nakamura and Hiroshi Kamiya

Additional information is available at the end of the chapter

http://dx.doi.org/10.5772/intechopen.75177

Abstract

Lakes Shinji and Nakaumi form a coupled brackish lake system on the Japan Sea coast of Japan, and seawater frequently intrudes into these lakes. The study analyzed the influence of river discharge, tide level, and meteorological forcing on seawater flux at Nakaura Watergate. Continuous wavelet transform (CWT), wavelet coherence (WTC), cross-wavelet transform (XWT), and partial wavelet coherence (PWC) were used to analyze seawater intrusion. CWT reveals the characteristics of seawater flux, river discharge, tide level, and meteorological forcing. WTC and XWT showed the correlation between forcing variables and seawater flux. PWC analyzed the impact of river discharge, tide level, and meteorological forcing variables on seawater flux after controlling the effect of all other forcing variables. The results showed that tide level has an impact on seawater flux over 0.5-day and 1-day cycle throughout the analysis period, suggesting that astronomical tides play an important role in the salinity intrusion processes. The river discharge characteristics and its influence on seawater flux were clearly revealed especially during high river flows. Sometimes, atmospheric pressure and wind velocity affect tide level, thereby driving salinity transport. The study reveals the power of wavelet analysis in examining nonlinear time series such as salinity intrusion processes.

Keywords: seawater flux, coastal lakes, wavelet analysis, wavelet coherence

1. Introduction

The wavelet transform has been used for process understanding since the early 1980s. It originated in geophysics and was significantly developed, both theoretically and application-oriented, in the signal processing and mathematics community [1]. Wavelets enable linear and

optimal extraction of information from a time series of any length [2]. The continuous wavelet transform (CWT) provides redundant information by mapping a time series into a function of time and frequency. The discrete wavelet transform (DWT) computes the transform for discrete values for time and frequency [3]. Hence, DWT is simple, easy to implement, and has low computational requirements. CWT requires a high computational time; however, it allows a larger freedom in wavelets selection than DWT. Redundant information in pictures from the CWT makes it easier to interpret results from the analysis of dynamic time series data. For an analysis where the main purpose is to reveal patterns or hidden information and data compression is not of concern, then redundancy provided by CWT may be useful [3]. Generally, CWTs are useful for dynamical analyses, while DWTs are better for information compression [2, 3].

This study utilized the CWT rather than DWT. The CWT may use an arbitrary number of *daughter wavelets* built from *mother wavelet* to match salinity oscillation periods, as needed for the optimal extraction of information concerning astronomical and meteorological forcing of the salinity intrusion. The *daughter wavelets* will be complete but not orthogonal. A DWT can be complete and orthogonal, given that it is built from functions with geometrically spaced periods; however, it may not have frequency flexibility necessary for salinity intrusion analysis [2].

Various studies have used wavelet analysis to analyze nonstationary time series water quality, meteorological, and hydrological data. Torrence and Compo provided a practical guide to wavelet analysis and also analyzed time series of the El Niño-Southern Oscillation (ENSO) [4]. Liu et al. ratified the bias problem in the estimation of the wavelet power spectrum and applied wavelet analysis to Niño-3 SST data [5]. Wavelet analysis was also used to study water-quality parameters [6, 7]. Zhang et al. [8], Sovi et al. [9], and Somoza et al. [10] used wavelet analysis to characterize water level variation. A number of studies have analyzed tidal variation and its influence on rivers using wavelet analysis [2, 11–13]. Ideião et al. studied the variability of the total monthly rainfall with the aid of CWT [4, 14]. The cross-wavelet transform (XWT) and wavelet coherence (WTC) techniques were used to analyze geophysical time series, for example, the effects of tidal range and river discharge on the salinity intrusion [15, 16], the impacts of Arctic Oscillation index and ENSO on the Baltic sea ice [17, 18], the relative humidity, and the shortwave radiation dataset [19]. Partial wavelet coherence (PWC) and multiple wavelet coherence (MWC) were used to study the impact of ENSO on the variability of tropical cyclones [20]. Wavelet analysis has also been applied in economics field [3, 21].

This study used CWT to analyze the period characteristics of tide level, river discharge, meteorological forcing variables, and seawater flux. It also quantified the relationships between river discharge, tide and meteorological forcing variables, and salinity intrusion, using WTC, XWT, and PWC. Several studies examined the effects of river discharge, tidal range, and meteorological forcing on salinity intrusion [15, 16]. Meteorologically induced sea surface variation (MISSV) and large periodic river discharge are considered to be effective water exchange mechanism between Lakes Nakaumi and Shinji, and the Japan Sea [22]. Though tidal amplitude on the Japan Sea is small, astronomical tides appear to be an effective water exchange mechanism [16]. The study of the influence of external forces on salinity

intrusion is difficult; the same applies to the development and application of seawater intrusion countermeasures. However, understanding the dynamic characteristics of forcing mechanisms and their influence on seawater intrusion enable the development and implementation of appropriate mitigation measures, for example, the regulation of river flow or the operation of flood control gates.

The previous wavelet analysis of salinity intrusion in the Sakai Channel was studied for one summer season [16]. Since salinity intrusion varies with season and time, the assessment of its dynamics requires a long-term analysis. Therefore, in order to understand the nonlinear characteristics of salinity intrusion in Sakai Channel in other seasons, this study conducted long-term wavelet analysis.

2. Materials and methods

2.1. Study area

Lakes Shinji and Nakaumi form a coupled brackish lake system in the western part of Japan (**Figure 1**). Lake Shinji has an average depth of 4.5 m, a surface area of 80 km^2, and a volume of 0.366 km^3. Lake Nakaumi has an average depth of 5.4 m, a surface area of 86.2 km^2, and a volume of 0.47 km^3. The Ohashi River (7.0 km long) connects the two lakes and the Sakai Channel (7.5 km long) connects Lake Nakaumi to the Japan Sea. The Hii River at the west-end of Lake Shinji supplies the lake system with most of its fresh water. Lake Shinji is a mesohaline lake with an average salinity between 1 and 6 PSU. Lake Nakaumi has a strongly differentiated two-layer system; the salinity of the surface water is 14–20 PSU and that of the bottom layer is 25–30 PSU. Hence, these brackish lakes are stably stratified due to salinity (density) differences, and density gradients have a large impact on water movement in this system [23].

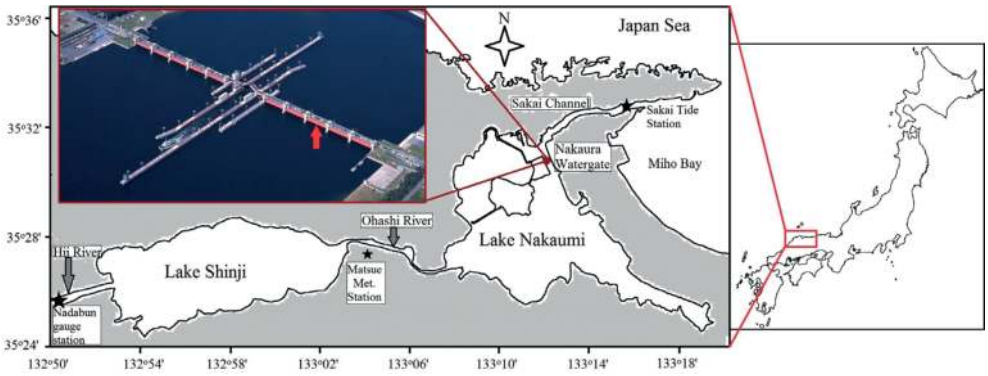

Figure 1. Location of Lakes Shinji and Nakaumi, and Nakaura Watergate monitoring station (insert). The red arrow indicates the third eastern-side floodgate, the location of sampling, and measurement equipment. Also shown are meteorological and hydrological monitoring stations (source: [16]).

2.2. Observations

Salinity data used in the study were collected at Nakaura Watergate monitoring station shown in **Figure 1**. Nakaura Watergate (width 414 m, depth 6.8 m) had five floodgates in the east and in the west (each 32 m long), and three floodgates at the center. On the western pile of the third east-side floodgate (indicated by a red arrow, **Figure 1**), submerged water pumps were installed for water sampling at 1, 2, 4, and 6 m from the bottom. The water was pumped to acrylic boxes in the floodgate administration building, where water temperature, electrical conductivity, and dissolved oxygen were measured every 30 min using custom-made sensors (Alec Electronics Co., Ltd.). Salinity was calculated from electrical conductivity.

Continuous measurements of salinity over a period of 6 years (February 1998 to March 2004) are available, although there are periods with missing data. Instantaneous seawater flux for the period January 2001 to October 2003 was used in this study. The salinity data were averaged to a 1-h interval to match the intervals of the other data used in the analysis. One-hour interval meteorological data (atmospheric pressure, wind speed, and direction) were collected at Matsue Meteorological Station (available on Japan Meteorological Agency website, http://www.jma.go.jp/jma/index.html). The wind was treated as a mathematical vector, and the mathematical convention for the direction was used, that is, wind direction was converted from "meteorological direction" to "math direction." The wind vector was resolved into its u (wx) and v (wy) components. Wind from the west was denoted as positive u and from the south a positive v. Tidal data used were recorded at Mihonoseki tide gauge station, and river discharge was recorded in Hii River at Nadabun gauging station (available on Japan's water information system website, http://www1.river.go.jp/).

2.3. Methodology

2.3.1. Salinity transport

Instantaneous advective salt transport (M_s, kg $m^{-1}s^{-1}$) per unit width of a section, normal to the longitudinal flow of the channel, is given by the following expression [24, 25]:

$$M_s = \int_0^h \rho VS dz = \overline{\rho VS} \cdot h \tag{1}$$

where ρ is the density, V is the longitudinal velocity component, and S is the longitudinal salinity. The upper bar denotes averaging over the total depth of the water column, h.

The study lakes are shallow. Pressure variation in shallow lakes is negligible. Therefore, the density of water was calculated using the following approximate density formula neglecting pressure [26]:

$$\rho = 999.83 + 0.808S - 0.0708(1 + 0.068T)T - 0.003(1 - 0.012T)(35 - S)T \tag{2}$$

where T is the temperature in °C and S is the salinity in PSU.

2.3.2. Continuous wavelet transform (CWT)

CWT decomposes a time series into a time-frequency space and determines both the dominant modes of variability and their variation with time [4]. The wavelet is applied as a bandpass filter to the time, stretching it in time by varying its scale(s) and normalizing it to have a unit energy [8, 18].

A wavelet $\psi(t)$ is a function that oscillates around the t-axis and loses strength as it moves away from the center, behaving like a small wave [4]. Beginning with a mother wavelet ψ, a family of "daughter wavelet" $\psi(\tau, s)$ is computed by scaling and translating ψ [4]:

$$\psi_{\tau,s}(t) = \frac{1}{\sqrt{|s|}}\psi\left(\frac{t-\tau}{s}\right); s, \tau \in \mathbb{R}; s \neq 0 \tag{3}$$

where $\psi(t)$ is the mother wavelet, $\psi_{\tau,s}(t)$ is the daughter wavelet, t is a nondimensional "time" parameter, s is a scaling or a dilation factor that controls the width of the wavelet, and τ is a translation parameter controlling the location of the wavelet.

This study used the Morlet wavelet, which consists of a plane wave modulated by a Gaussian or in other words a complex exponential function multiplied by a Gaussian window. Hence, it represents the best compromise between frequency and time localization. A complex wavelet is essential for this study, as it yields a complex transform, with information on both the amplitude and the phase, crucial to study the synchronization of oscillations between different time series [3, 27]. Morlet wavelet is defined as [4]

$$\psi_0(t) = \pi^{-1/4} e^{i\omega_0 t} e^{-t^2/2} \tag{4}$$

where $\psi_0(t)$ is the Morlet wavelet, ω_0 is the fundamental frequency, which gives the number of oscillations within the wavelet itself.

CWT of a time series $x(t) \in L^2(\mathbb{R})$ with respect to the wavelet ψ is a function of two variables, $W_{x;\psi}(\tau, s)$ [3]:

$$W_{x;\psi}(\tau, s) = \int_{-\infty}^{\infty} x(t) \frac{1}{\sqrt{|s|}} \psi^*\left(\frac{t-\tau}{s}\right) dt \tag{5}$$

where $W_{x;\psi}(\tau, s)$ is the CWT of a time series $x(t)$, $L^2(\mathbb{R})$ denotes the set of square integrable functions, that is, the set of functions defined on the real line and satisfying $\int_{-\infty}^{\infty} |x(t)|^2 dt < \infty$, ψ^* is the complex conjugation of ψ.

2.3.3. Cross-wavelet transform (XWT)

The cross-wavelet transform (XWT), a multiscale signal analytical technique, combines the wavelet transform and cross-spectrum analysis. XWT analyzes multiple time-frequencies of

two time series from multiple time scale points, thereby exposing regions with a common high power, and further reveals information about the phase relationship in time-frequency space, hence determining correlations [15, 18].

For two time series x_n and y_n, their cross-wavelet transform is given by [4, 15]

$$W_n^{XY}(s) = W_n^X(s)W_n^{Y*}(s) \tag{6}$$

where $W_n^X(s)$ and $W_n^Y(s)$ are wavelet transforms of x_n and y_n, respectively, and * denotes complex conjugation. $\left|W_n^{XY}(s)\right|$ is the cross-wavelet power. If two time series have background power spectra P_k^X and P_k^Y, then their theoretical distribution of the cross-wavelet power is given by [4, 18].

$$D\left(\frac{\left|W_n^X(s)W_n^{Y*}(s)\right|}{\sigma_X\sigma_Y} < p\right) = \frac{Z_v(p)}{v}\sqrt{P_k^X P_k^Y} \tag{7}$$

where σ_X and σ_Y are the respective standard deviations, $Z_v(p)$ is the confidence level associated with the probability p for a probability distribution function (*pdf*) defined by the square root of the product of two chi-squared (χ^2) distributions.

2.3.4. Wavelet coherence (WTC)

Wavelet coherence (WTC) between two CWTs can find significant coherence even though the common power is low and show how confidence levels against red noise backgrounds are calculated. This can be thought of as a local correlation between two time series in the time-frequency space. It finds locally phase-locked behavior. The significance level of the WTC is determined using Monte Carlo methods [15]

$$R_n^2(s) = \frac{\left|S\left(s^{-1}W_n^{XY}(s)\right)\right|^2}{S\left(s^{-1}\left|W_n^X(s)\right|^2\right)\cdot S\left(s^{-1}\left|W_n^Y(s)\right|^2\right)} \tag{8}$$

where S is a smoothing operator.

2.3.5. Partial wavelet coherence

CWT is increasingly being used in the analysis of marine sciences time series data. However, most of the CWT analyses have been limited to univariate and bivariate analyses, that is, the wavelet power spectrum, the wavelet coherency, and the wavelet phase difference [3]. Wavelet analysis tools have already been extended to allow for multivariate analyses [3, 20]. PWC and PPD are the examples of recent wavelet analysis techniques. The PWC technique is similar to partial correlation and it identifies the resulting wavelet coherence between two time series after eliminating the influence of their common dependence [20]. The applicability of PWC to geophysics was demonstrated during the study of the "stand-alone" relationship between the

"ratio of number of typhoons to number of tropical cyclones" and "large-scale atmospheric factors" after removing the effect of El Nino-Southern Oscillation (ENSO) [20].

The squared multiple wavelet coherence ($R^2_{1(23\ldots p)}$) between the series x_1 and all the other series $x_2,\ldots, x_p$ is given by the following formula [3]:

$$R^2_{1(23\ldots p)} = 1 - \frac{C^d}{C^d_{11}} \tag{9}$$

where C denotes the $p \times p$ matrix of all the complex wavelet coherencies ϱ_{ij}, that is, $C = \left(\varrho_{ij}\right)_{i,j=1}^{p}$, $C^d = \det C$.

The complex partial wavelet coherence ($\varrho_{1j.q_j}$) of x_1 and $x_j (2 \leq j \leq p)$ allowing for all the other series is given by [3]

$$\varrho_{1j.q_j} = -\frac{C^d_{j1}}{\sqrt{C^d_{11}}\sqrt{C^d_{jj}}} \tag{10}$$

The partial wavelet coherence ($R_{1j.q_j}$) of x_1 and x_j allowing for all the other series is defined as the absolute value of Eq. (10), that is,

$$R_{1j.q_j} = \frac{\left|C^d_{j1}\right|}{\sqrt{C^d_{11}C^d_{jj}}} \tag{11}$$

and the squared partial wavelet coherence of x_1 and x_j allowing for all the other series is simply the square of $R_{1j.q_j}$.

The partial phase delay (phase difference) of x_1 and x_j given all the other series is defined as the angle of $\varrho_{1j.q_j}$. A complex wavelet function contains information about both the amplitude and the phase, making it suitable to capture oscillatory behavior. Complex partial wavelet coherence, $\varrho_{1j.q_j}$ considered can be separated into its real part, $\Re\left(\varrho_{1j.q_j}\right)$, and imaginary part, $\Im\left(\varrho_{1j.q_j}\right)$, or in its amplitude, $\left|\varrho_{1j.q_j}\right|$, and phase angle $\phi_{1j.q_j}$. The phase difference, $\phi_{1j.q_j}$, is given as follows [3]:

$$\phi_{1j.q_j} = Arctan\left(\frac{\Im\left(\varrho_{1j.q_j}\right)}{\Re\left(\varrho_{1j.q_j}\right)}\right) \tag{12}$$

A phase difference of zero indicates that the time series moves together at the specified time-frequency; if $\phi_{x_1x_j} \epsilon (0, 90)$, the series moves in a phase and the time series of x_1 leads x_j; if $\phi_{x_1x_j} \epsilon (-90, 0)$, then x_j leads x_1. A phase difference of 180 (or -180) indicates an antiphase

relationship; if $\phi_{x_1 x_j} \epsilon (90, 180)$, then x_j leads x_1; if $\phi_{x_1 x_j} \epsilon (-180, -90)$, then x_1 leads x_j (see **Figure 2**). Phase difference can be converted into instantaneous time lag between two time series by dividing the phase difference, $\phi_{1j.q_j}$ by the angular frequency corresponding to the scale s, $\omega(s)$.

2.3.6. Significance tests

It is important to assess the statistical significance of the wavelet, cross-wavelet power and the wavelet coherence. The assessment of the statistical significance levels and confidence intervals against red noise backgrounds was done using direct Monte Carlo simulations.

2.3.7. Wavelet packages and parameters used

Ng and Kwok provided the software for CWT, WTC, and XWT, which is available at http://www.cityu.edu.hk/gcacic/wavelet. It is used in collaboration with the software provided by Grinsted, which is available at http://www.glaciology.net/wavelet-coherence. The software for PWC was provided by Aguiar-Conraria and Soares and is available at http://sites.google.com/site/aguiarconraria/joanasoares-wavelets. Some of the parameters used in the analysis are as follows: the mother wavelet function—Morlet; the sampling time (dt)—1 h; the spacing between discrete scales (dj)—0.5 h; the level of significance—5%; and the number of Monte Carlo simulations used to assess statistical significance—1000. Default values were taken for other parameters.

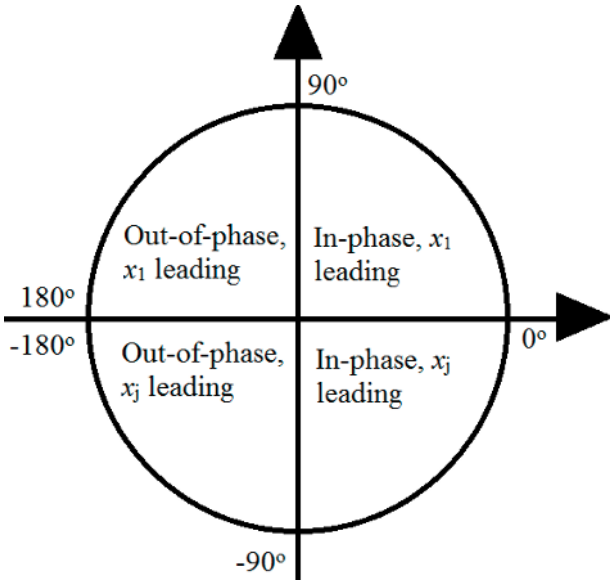

Figure 2. Phase difference circle.

http://dx.doi.org/10.5772/intechopen.75177

3. Results and discussion

3.1. Analysis of period characteristics

3.1.1. Variability of seawater flux

Figure 3 shows the seawater flux per unit width at Nakaura Watergate and its CWT coefficient chart. Positive values of the time series indicate seawater flux toward the Japan Sea and negative toward Lake Nakaumi. The CWT coefficient chart for seawater flux has stable period characteristics, with high power oscillations in the 12-h and 1-day period band throughout the analysis period. Both the red color and the black contour indicate that cycles are strong and statistically significant at 95% confidence level (hereinafter statistically significant).

3.1.2. Variability of tide level

Figure 4 shows time series plot and CWT coefficient chart for the tide level. The high-power tide level oscillations have statistically significant periods of 12 h and 1 day. This implies considerable power spreads throughout the semi-diurnal and diurnal bands throughout the analysis period. The oscillations indicate spring-neap tidal variations since they appear twice a month. Also observed is a relatively strong statistically significant, though not regular, 2–6-day period cycle that occurs mainly in winter (December to March). Tide level and atmospheric pressure are negatively correlated. The time series of both shows that as the atmospheric pressure increases, the tide level decreases and vice versa (**Figures 4** and **5**).

3.1.3. Variability of sea level atmospheric pressure

The CWT coefficient chart for the atmospheric pressure (**Figure 5**) shows continuous statistically significant high power 64-day period cycles from April 2002. There are also 128-day to 1-year period cycles throughout the analysis period. There are some discontinuous and irregular high power oscillations in the 1-day and 2–32-day period cycles.

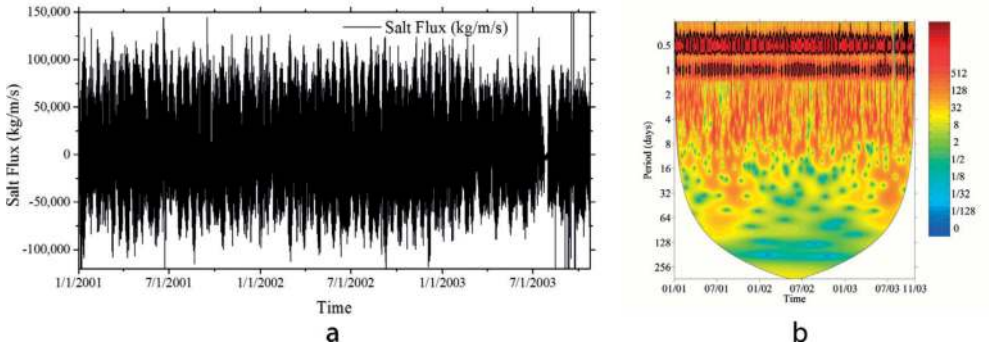

Figure 3. (a) The time series of salinity flux (salt flux (kg/m/s)) and (b) its wavelet power spectrum for the Jan 2001 to Oct 2003 period. Period is in days. The red color designates high power oscillations whilst blue is low power oscillations. The *black* contour designates 95% confidence level, using *red* noise as the background spectrum. *White* regions on either end indicate the "cone of influence" where edge effects become important.

3.1.4. Variability of river discharge

Figure 6 shows the time series plot and CWT coefficient chart for the total river discharge in Hii River. Wavelet coefficients acutely vary from the highest to the lowest, indicating an unstable river discharge. The chart also shows a distinct character that has long vertical peaks like a raindrop, which indicate that the period of oscillation varies from high to low almost

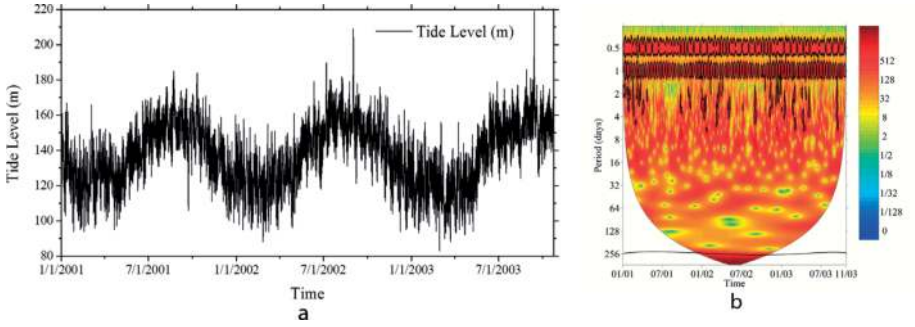

Figure 4. Tide level—time-series plot (a) and time-series wavelet power spectrum (b) for the Jan 2001 to Oct 2003 period.

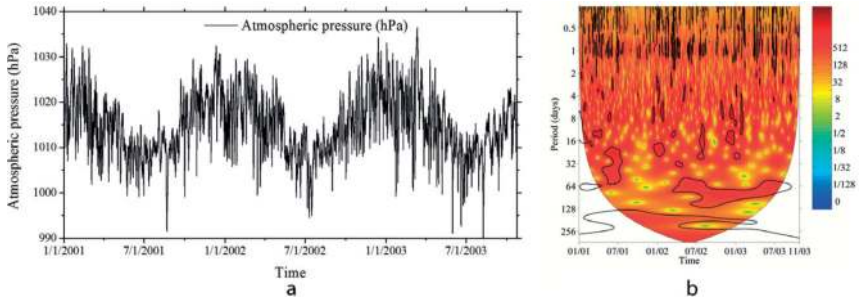

Figure 5. Atmospheric pressure–time-series plot (a) and time-series wavelet power spectrum (b) for the Jan 2001 to Oct 2003 period.

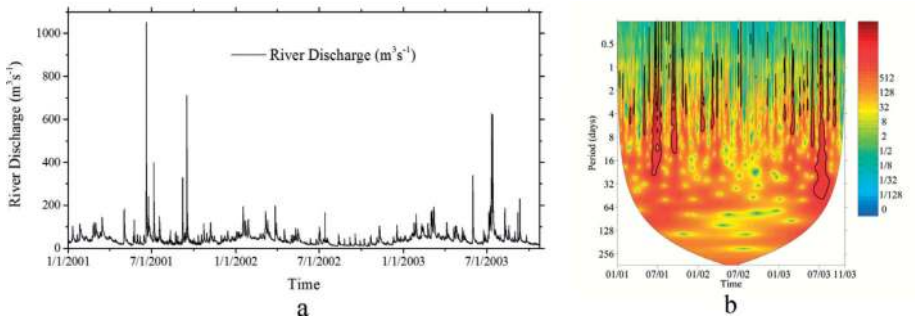

Figure 6. River discharge—time-series plot (a) and time-series wavelet power spectrum (b) for the Jan 2001 to Oct 2003 period.

instantaneously. Each peak of energy corresponds to a high river discharge. From the time series plot and CWT coefficient chart, it is evident that the highest river flow rate occurs in June and July. However, there were little rains in the summer of 2002 compared to that of 2001 and 2003. The CWT coefficient chart did show the river discharge in the summer of 2002 as significant; however, the wavelet analysis of the periods June–September 2002 indicated high energy in June and July [16]. The river discharge during June–July 2002 was dwarfed by that of June–July 2001 and 2003 and hence the absence of high energy on the CWT coefficient chart.

3.1.5. Variability of wind velocity

Figure 7 shows the CWT coefficient chart for the wind velocity vectors. There are observations of fluctuating medium power in the 0.5-day period band for the North–South (*wy*) wind velocity component throughout the analysis period. The strong and statistically significant oscillations are in the 2–14-day period band throughout the analysis period. The East–West (*wx*) wind velocity component has discontinuous and irregular high power oscillations in the 2–16-day period band. There are continuous medium-power oscillations in the 32-day period band and 64-day to 1-year period band.

3.2. Analysis of dynamic relationships

3.2.1. Correlation between the tide level and the seawater flux

The WTC and XWT of the tide level and the seawater flux are shown in **Figure 8**, which displays that significant power sections appear continuously throughout the analysis period. This indicates

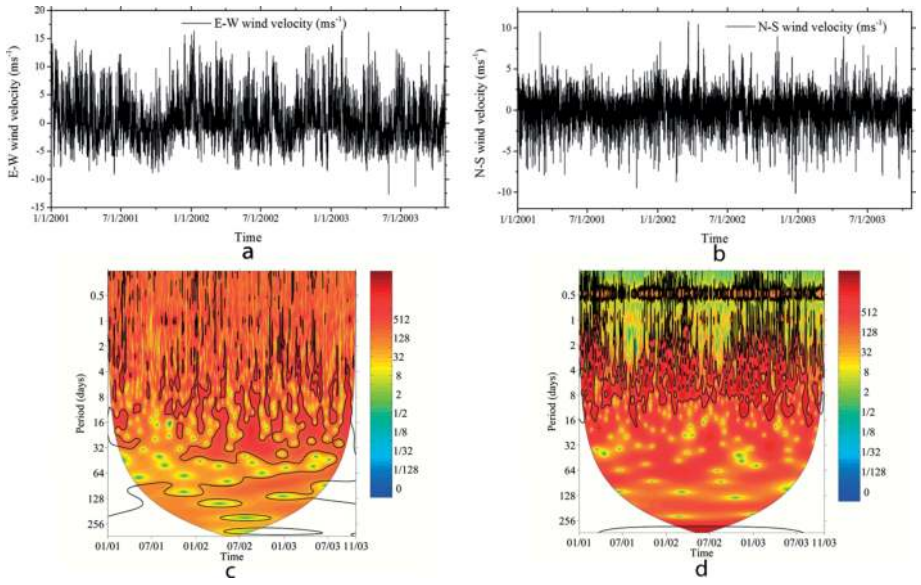

Figure 7. Wind velocity (*wx* (a & c) and *wy* (b & d))—time-series plot (a & b) and time-series wavelet power spectrum (c & d) for the Jan 2001 to Oct 2003 period.

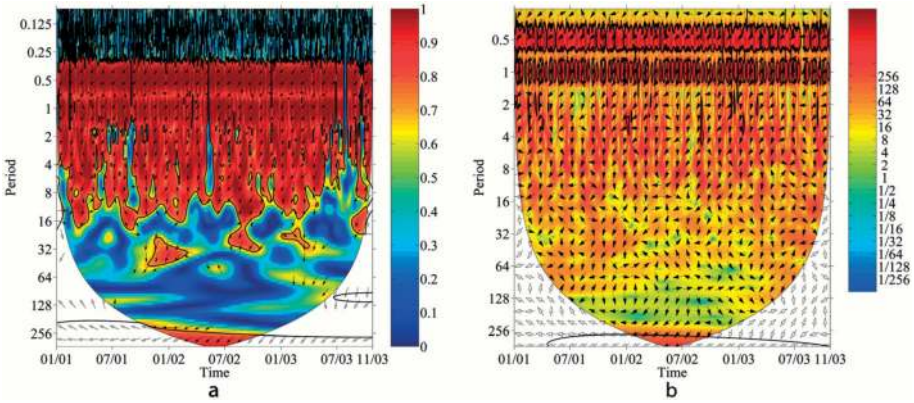

Figure 8. The WTC (a) and XWT (b) of the tide level and the salinity flux for the Jan 2001 to Oct 2003 period. The arrows represent phase difference. The arrow pointing up and to the right—in-phase relationship with the tide level leading. The arrow pointing down and to the left—out-of-phase relationship with the tide level leading.

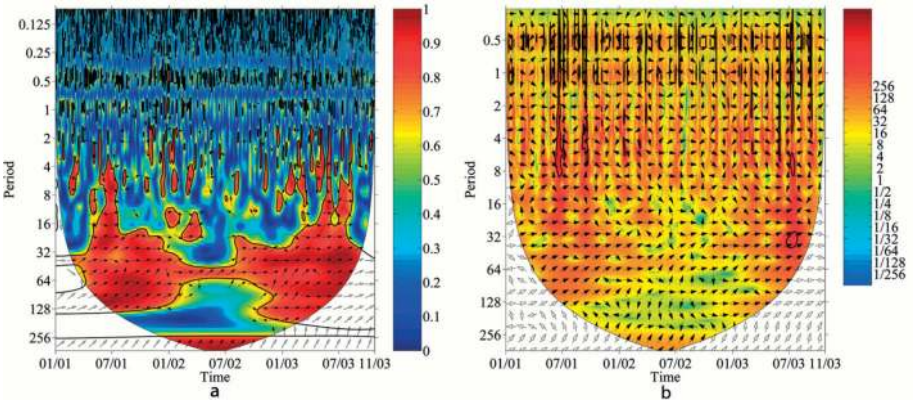

Figure 9. The WTC (a) and XWT (b) of river discharge and salinity flux for the Jan 2001 to Oct 2003 period.

that the influence of the tide level on the seawater flux is strong. Both WTC and XWT show significant power sections in the semi-diurnal and diurnal periods. WTC also shows almost continuous coherence between the tide level and the seawater flux in the 2–16-day period band. XWT does not show much common power in the 2–16-day period band. This indicates that the tide level influences the seawater flux mainly in the 0.5-day and 1-day period band. Both WTC and XWT show that in the 0.5-day and 1-day period band, the tide level and the seawater flux have an antiphase relationship with tides leading (the arrow pointing down and to the left). That is, a rise in the tide level leads to an increase in the negative seawater flux (seawater flux into Lake Nakaumi is denoted as the negative flux in this study).

3.2.2. Correlation between the river discharge and the seawater flux

Extensive significant power sections show the influence of river discharge on salinity, **Figure 9**. The WTC shows continuous coherence in the 16–128-day period band and discontinuous

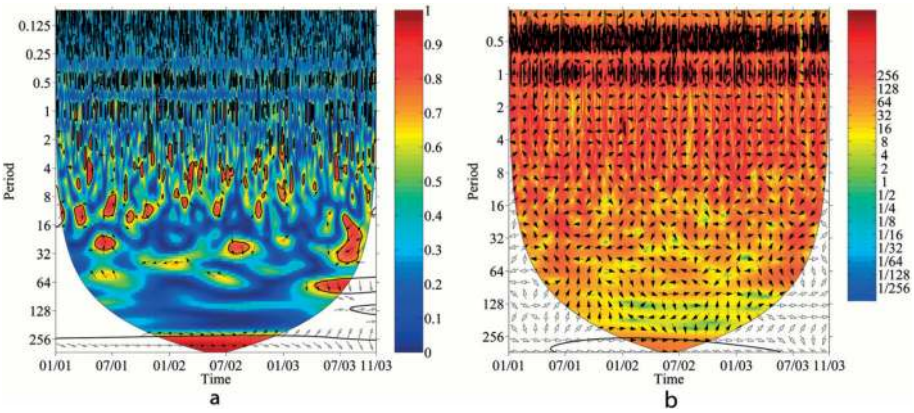

Figure 10. The WTC (a) and XWT (b) of the atmospheric pressure and the salinity flux for the Jan 2001 to Oct 2003 period.

coherence in the 2–16 period band. However, the XWT shows the occasional appearance of the significant power sections with irregular intervals especially during the summer period. The power section appears around June, July, September, and January. The influence of the river discharge on the seawater flux failed to pass the significance test at 5% level in other months and the summer of 2002.

3.2.3. Correlation between the atmospheric pressure and the seawater flux

The XWT and WTC of the atmospheric pressure and the seawater flux shown in **Figure 10** occasionally display extensive significant power sections in the 0.5-, 1–, and 256-day to 1-year period band, which stands out throughout analysis period, testing the existence of the correlation between the atmospheric pressure and the seawater flux. The WTC shows occasional correlation in the 2–16-day period band.

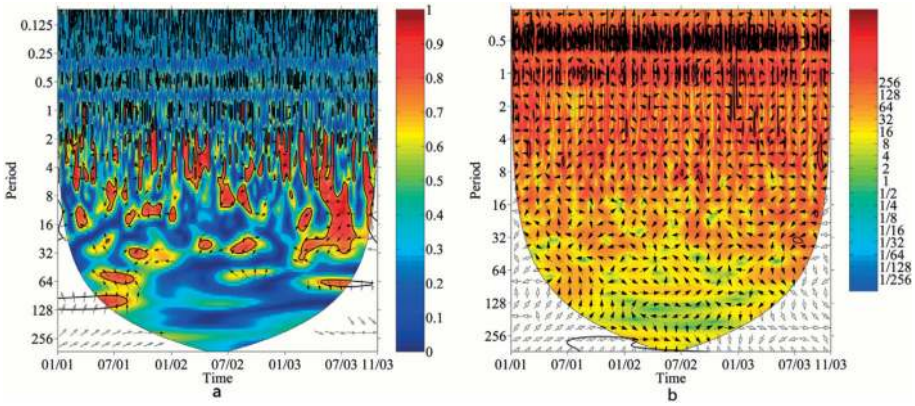

Figure 11. The WTC (a) and XWT (b) for the *wx* wind velocity component and salinity flux for the Jan 2001 to Oct 2003 period.

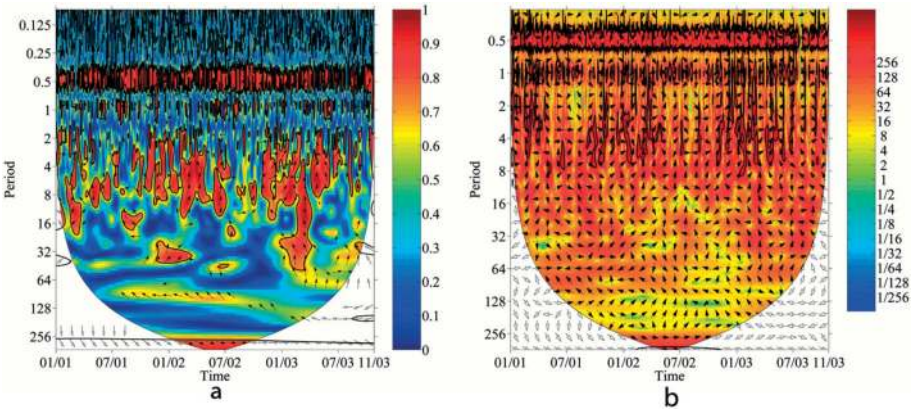

Figure 12. The WTC (a) and XWT (b) for the *wy* wind velocity component and salinity flux for the Jan 2001 to Oct 2003 period.

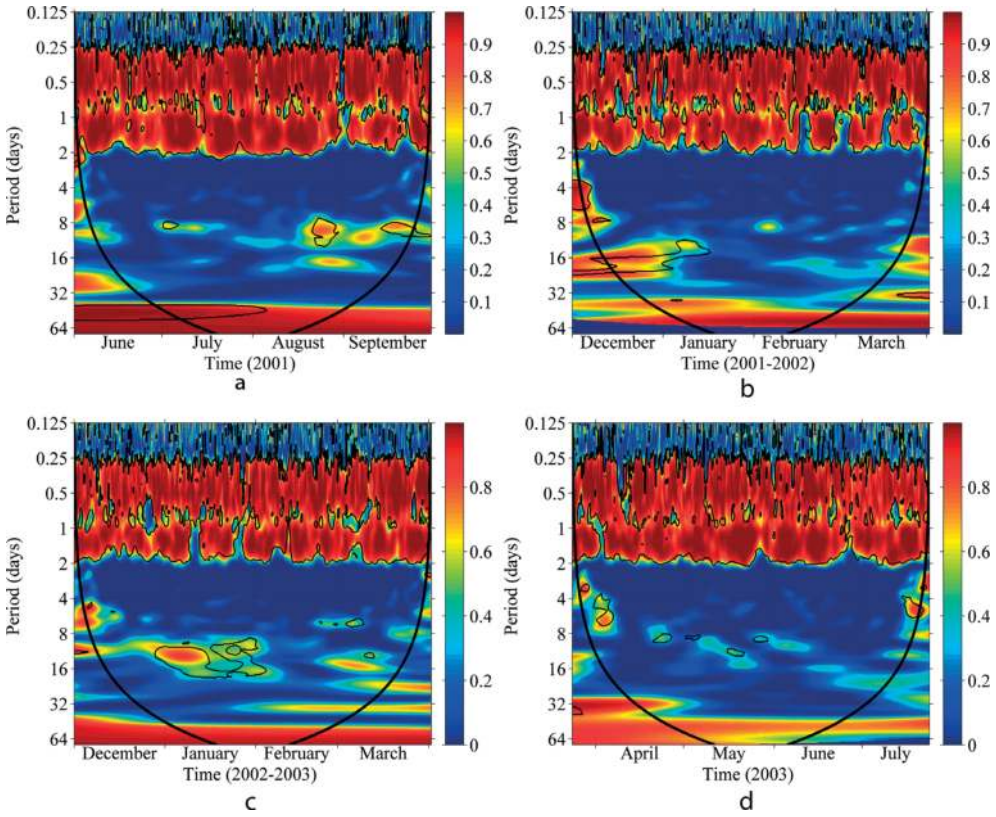

Figure 13. Partial wavelet coherence of observed tides versus salinity flux for the period (a) Jun-Sep 2001, (b) Dec 2001 - Mar 2002, (c) Dec 2002 - Mar 2003, (d) Apr-Jul 2003. The thick black line indicates the cone of influence that delimits the region not influenced by edge effects.

3.2.4. Correlation between the wind velocity and the seawater flux

The XWT and WTC for the wind velocity vectors and the seawater flux are shown in **Figures 11** and **12**. East–West (*wx*) wind velocity vector also influences seawater flux. The WTC indicates significant discontinuous and irregular power sections on the periods 2–32 days throughout the statistical intervals as shown in **Figure 11**. The XWT shows some discontinuous and irregular significant power sections in the 0.5- and 1-day period band, testifying that sometimes a correlation exists between East–West wind velocity component and seawater flux.

The XWT and WTC for North–South (*wy*) wind velocity vector display continuous extensive significant power sections, and their center focuses on the period of 0.5 day (**Figure 12**). The significant power sections also appear at irregular intervals with varying periods in the 2–16-day period band. Powerful influence of wind speed is consistent in the 0.5 day throughout the analysis period.

3.3. Analysis of dynamic characteristics using partial wavelet coherence

Figures 13–17 shows PWC, the relationship, in the time-frequency domain, between seawater flux and each of the forcing variables, after eliminating the effect of other variables. Two summer

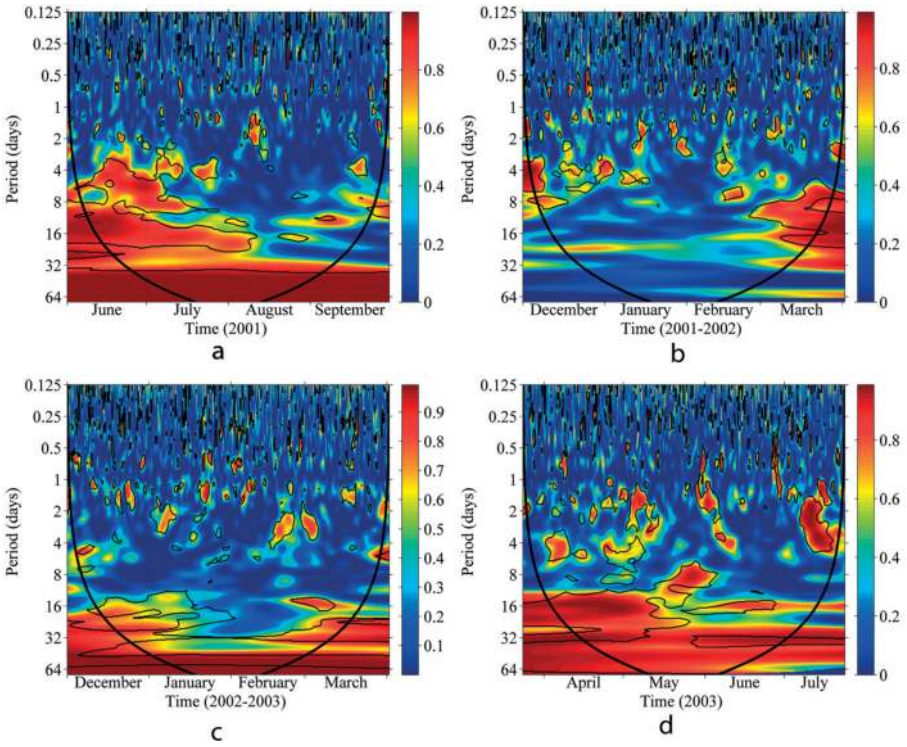

Figure 14. Partial wavelet coherence of river discharge versus salinity flux for the period (a) Jun-Sep 2001, (b) Dec 2001 - Mar 2002, (c) Dec 2002 - Mar 2003, (d) Apr-Jul 2003.

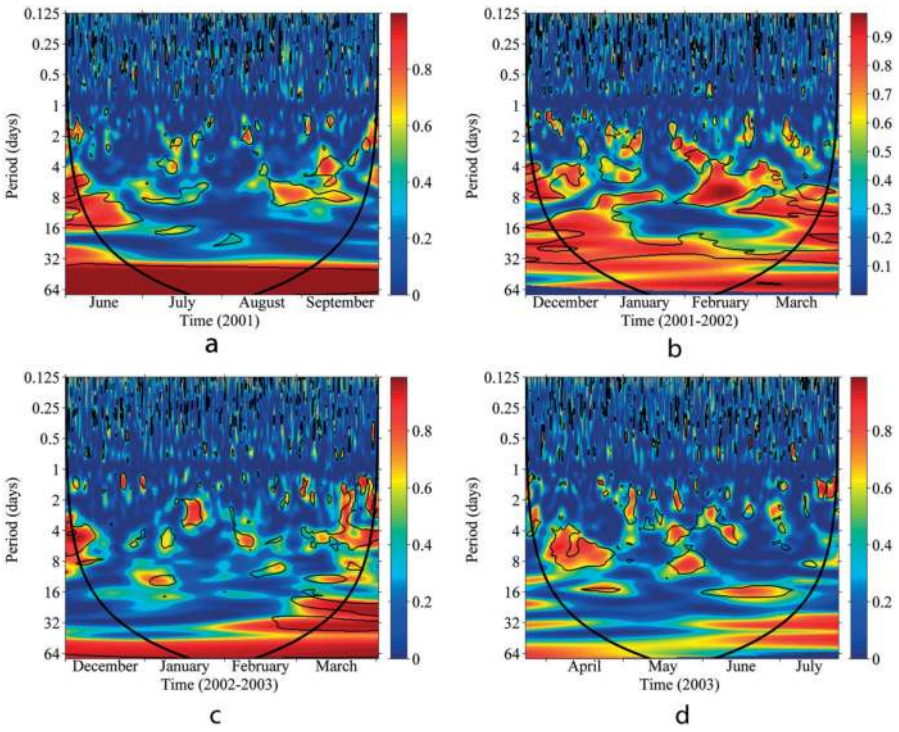

Figure 15. Partial wavelet coherence of atmospheric pressure versus salinity flux for the period (a) Jun-Sep 2001, (b) Dec 2001 - Mar 2002, (c) Dec 2002 - Mar 2003, (d) Apr-Jul 2003.

seasons and two winter seasons were analyzed separately in order to visualize the relationships that might otherwise be lost in a long-term analysis. The analysis of 2002 summer season was done before and will be compared with the current analysis [16].

3.3.1. PWC between the tide level and the seawater flux

Figure 13 shows extensive statistically significant coherence at the 5% level in all the seasons, indicating the existence of relationship between observed tides and salinity transport. The center of power sections focuses on periods 0.5 and 1 day. Tides have a positive impact on seawater flux over the periods 0.5 and 1 day throughout the year. This study reinforces previous conclusion that short-term salinity transport is highly influenced by tides [16].

3.3.2. PWC between the river discharge and the seawater flux

PWC between the river discharge and the seawater flux, after controlling for other forcing variables, shows statistically significant in-phase relationship in the 3–16-day period in all the seasons analyzed (**Figure 14)**. The 2001 summer (June and July) and spring/summer 2003 (April–June) show a significant continuous coherence between the river discharge and the seawater flux in the 16-day period band. In July 2003, though the coherence in the 16-day band

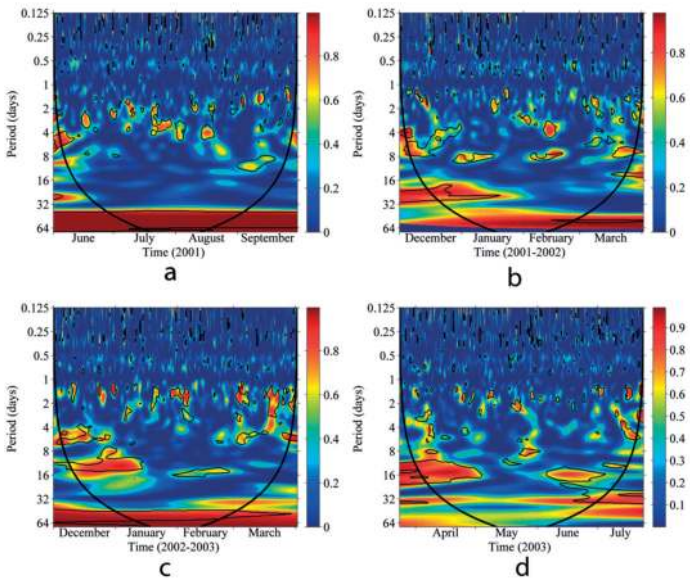

Figure 16. Partial wavelet coherence of East–West (*wx*) wind velocity component versus salinity flux for the period (a) Jun-Sep 2001, (b) Dec 2001 - Mar 2002, (c) Dec 2002 - Mar 2003, (d) Apr-Jul 2003.

is high, it is not statistically significant. The winter periods also showed some significant correlation between the river discharge and the seawater flux. 2001–2002 winters have coherences, which are discontinuous and occur at irregular intervals. March 2002 exhibits a significant continuous coherence in the 4–24-day period band. 2002–2003 winters have statistically significant coherences that occur continuously in the 16–32-day period band. This shows the existence of the relationship between the river discharge and the seawater flux, which generally coincides with an increased river discharge. The effect of increased river flows due to rain, typhoon events, and water releases upstream is clearly shown.

3.3.3. PWC between the atmospheric pressure and the seawater flux

During summer, a discontinuous and irregular statistically significant relationship between the atmospheric pressure and the seawater flux exists in the 4–16-day period band, indicating the existence of an on-and-off correlation between the tide level and the seawater flux (**Figure 15**). During winter, a continuous relationship exists in the 16–32-day period band. WTC and XWT show that the atmospheric pressure's influence on the flux of seawater is not stable, implying that it is short-lived and has a weak influence on seawater flux (**Figure 10**). However, PWC shows that the atmospheric pressure sometimes influences the seawater flux.

3.3.4. PWC between the wind velocity and the seawater flux

Figures 16 and **17** show partial wavelet coherence between the wind velocity and the seawater flux. An unstable relationship between wind vectors and seawater flux is exhibited. The East–West (*wx*) wind velocity component and seawater flux have a discontinuous and irregular

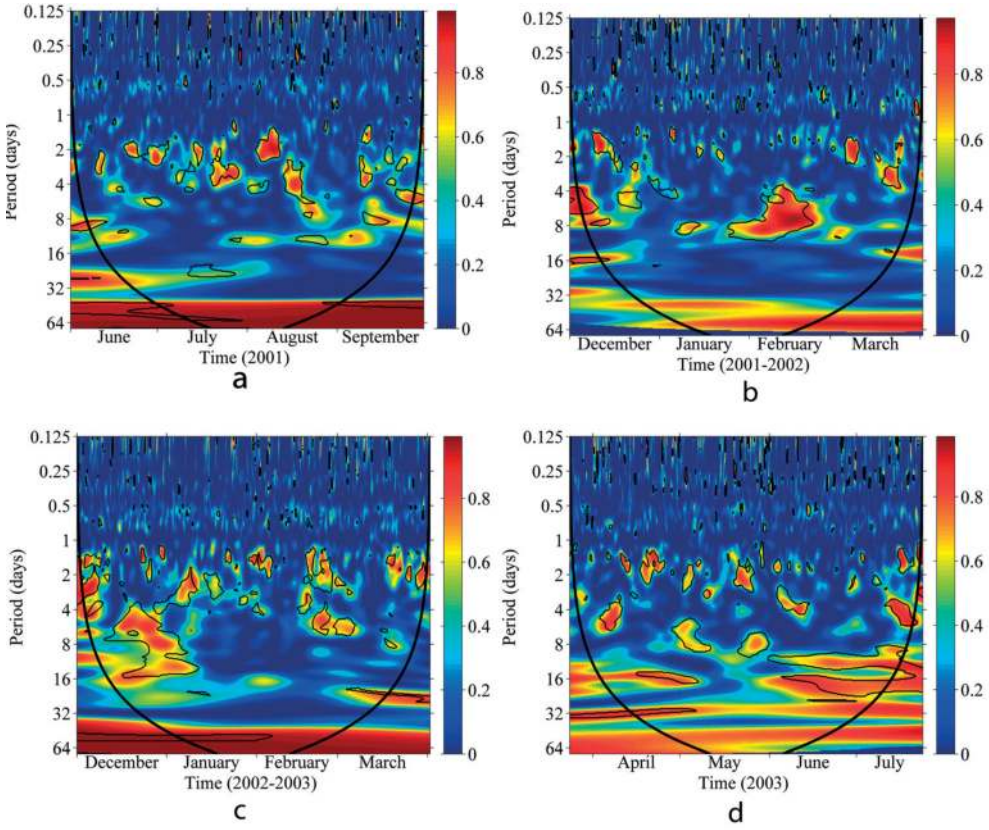

Figure 17. Partial wavelet coherence of North–South (*wy*) wind velocity component versus salinity flux for the period (a) Jun-Sep 2001, (b) Dec 2001 - Mar 2002, (c) Dec 2002 - Mar 2003, (d) Apr-Jul 2003).

relationship, mainly in the periods between 2 and 8 days. A continuous month-long relationship exists in the 8–16-day period band. The statistically significant month-long power sections for the North–South (*wy*) wind velocity component exist for 2001–2002 winters, 2002–2003 winters, and 2003 summer. The statistically significant correlation between the North–South (*wy*) wind velocity component and seawater flux exists mainly in the 2–16-day period band. Short-term oscillations are irregular and short-lived.

4. Conclusion(s)

This study explored the usefulness of continuous wavelet analysis in the investigation of salinity intrusion. The study summarized CWT, WTC, XWT, and PWC approaches and applied them in the analysis of the impact of forcing variables on the seawater flux in Sakai Channel. The study

revealed fundamental characteristics in the variation of forcing parameters and seawater flux, as well as their interactions. The only constraint in this study was a high computation time due to 1000 Monte Carlo simulation runs.

The CWT results show that the seawater flux and the tide level have regular oscillations in the 12-h and 1-day period band, indicating that the influence of astronomical tides is dominant. River discharge from the Hii River does not exhibit any periodical variations due to the irregularity of precipitation and the controlled release from upstream reservoirs. Atmospheric pressure exhibits a continuous high power (lasting over a month) with a period range from 16-day to 1-year. East–West (*wx*) and North–South (*wy*) wind velocity components show irregular oscillations with periods between 2 and 16 days.

WTC, XWT, and PWC revealed the influence of tide level, river discharge, atmospheric pressure, and wind velocity on seawater flux. WTC, XWT, and PWC showed that tides are consistently influential on the seawater flux in the 0.5- and 1-day period band. River discharge influenced seawater flux after heavy rains or water releases from upstream reservoirs. Atmospheric pressure and wind velocity occasionally influence seawater flux at Nakaura Watergate and may have an indirect influence on salinity transport through their effect on sea surface elevation. High drops of atmospheric pressure occasionally resulted in an increased tide level. This study reiterated the importance of tides in the transport of seawater in and out of Lakes Shinji and Nakaumi.

To conclude, the wavelet analysis of seawater intrusion studies proved useful. Wavelet coherence is helpful in the study of relationships between two time series. Partial wavelet coherence reveals the relationship between two time series after removing the effect of other time series. This is very useful when a dependent variable is under the influence of two or more variables. Wavelet analysis performs spectral analysis in frequency-time domain, revealing time-varying relationships across frequencies.

Acknowledgements

Shimane Prefectural Institute of Public Health and Environmental Science provided the salinity, water temperature, and current velocity data used in this study.

Author details

Edwin Muchebve[1]*, Yoshiyuki Nakamura[1] and Hiroshi Kamiya[2]

*Address all correspondence to: muchebve-edwin-tg@ynu.jp

1 Graduate School of Urban Innovation, Yokohama National University, Yokohama, Japan

2 Research Centre for Coastal Lagoon Environments, Shimane University, Matsue, Japan

References

[1] Kumar P, Foufoula-Georgiou E. Wavelet analysis for geophysical applications. Reviews of Geophysics. 1997;**35**(4):385

[2] Flinchem EP, Jay DA. An introduction to wavelet transform tidal analysis methods. Estuarine, Coastal and Shelf Science. 2000 Aug;**51**(2):177-200

[3] Aguiar-Conraria L, Soares MJ. The continuous wavelet transform: Moving beyond uni- and bivariate analysis. Journal of Economic Surveys. 2014;**28**(2):344-375

[4] Torrence C, Compo GP. A practical guide to wavelet analysis. Bulletin of the American Meteorological Society. 1998 Jan;**79**(1):61-78

[5] Liu Y, San Liang X, Weisberg RH. Rectification of the bias in the wavelet power spectrum. Journal of Atmospheric and Oceanic Technology. 2007 Dec;**24**(12):2093-2102

[6] Parmar KS, Bhardwaj R. Wavelet and statistical analysis of river water quality parameters. Applied Mathematics and Computation. 2013 Jun;**219**(20):10172-10182

[7] Shaharuddin M, Zaharim A, Nor MJM, Karim OA, Sopian K. Using wavelet transform on suspended particulate matter (PM10) and meteorological time series. In: Proceedings of the 12th WSEAS International Conference on Applied Mathematics. World Scientific and Engineering Academy and Society (WSEAS); 2007. pp. 179-183

[8] Zhang Q, Xu C-Y, Chen YD. Wavelet-based characterization of water level behaviors in the Pearl River estuary, China. Stochastic Environmental Research and Risk Assessment. 2009 Jan 13;**24**(1):81-92

[9] Sovi A, Poto K, Serši D, Kuspili N. Wavelet analysis of hydrological signals on an example of the River Sava. In: MIPRO, 2012 Proceedings of the 35th International Convention; Opatija, Croatia: IEEE; 2012. pp. 1223-1228

[10] Somoza RD, Pereira ES, Novo EML, Rennó CD. A water level relationship between consecutive gauge stations along Solimoes/Amazonas main channel: A wavelet approach. 2013 Oct;**178**:53-62

[11] Briciu A-E. Wavelet analysis of lunar semidiurnal tidal influence on selected inland rivers across the globe. Scientific Reports. 2014 Jan;**4**:4193

[12] Briciu A-E. Supplementary Information—Wavelet analysis of lunar semidiurnal tidal influence on selected inland rivers across the globe. Scientific Reports. 2014;**4**:4193

[13] Lim Y-H, Lye LM. Wavelet analysis of tide-affected low streamflows series. Journal of Data Science. 2004;**2**:149-163

[14] Ideião SMA, Santos CAG. Analysis of precipitation time series using the wavelet transform. Sociedade & Natureza. 2005 May;**1**(1):736-745

[15] Liu B, Yan S, Chen X, Lian Y, Xin Y. Wavelet analysis of the dynamic characteristics of saltwater intrusion—A case study in the Pearl River Estuary of China. Ocean and Coastal Management. 2014 Jul;**95**:81-92

[16] Muchebve E, Nakamura Y, Suzuki T, Kamiya H. Analysis of the dynamic characteristics of seawater intrusion using partial wavelet coherence: A case study at Nakaura Watergate, Japan. Stochastic Environmental Research and Risk Assessment. 2016 Dec 31;**30**(8):2143-2154

[17] Jevrejeva S, Moore JC, Grinsted A. Influence of the Arctic oscillation and El Niño-Southern oscillation (ENSO) on ice conditions in the Baltic Sea: The wavelet approach. Journal of Geophysical Research—Atmospheres. 2003 Nov 16;**108**(D21):4677

[18] Grinsted A, Moore JC, Jevrejeva S. Application of the cross wavelet transform and wavelet coherence to geophysical time series. Nonlinear Processes in Geophysics. 2004;**11**(5/6): 561-566

[19] Veleda D, Montagne R, Araujo M. Cross-wavelet bias corrected by normalizing scales. Journal of Atmospheric and Oceanic Technology. 2012;**29**(9):1401-1408

[20] Ng EKW, Chan JCL. Geophysical applications of partial wavelet coherence and multiple wavelet coherence. Journal of Atmospheric and Oceanic Technology. 2012;**29**(12):1845-1853

[21] Mandler M, Scharnagl M. Money growth and consumer price inflation in the euro area: A wavelet analysis. Discussion Paper. Deutsche Bundesbank; 2014. Report No.: 33/2014

[22] Nakata K, Horiguchi F, Yamamuro M. Model study of Lakes Shinji and Nakaumi—A coupled coastal lagoon system. Journal of Marine Systems. 2000 Oct;**26**(2):145-169

[23] Okuda S. Water movement and physical environments in brackish lakes—Shinjiko and Nakaumi. In: International Seminar on Restoration of Damaged Lagoon Environments; Matsue, Japan; 2004. pp. 1-6

[24] Vaz N, Lencarte Silva JD, Dias JM. Salt fluxes in a complex river mouth system of Portugal. PLoS One. 2012 Oct 10;**7**(10):e47349

[25] Moser GAO, Gianesella SMF, Barrera-Alba JJ, Bérgamo AL, Saldanha-Corrêa FMP, De Miranda LB, et al. Instantaneous transport of salt, nutrients, suspended matter and Chlorophyll-a in the tropical estuarine system of Santos. Brazilian Journal of Oceanography. 2005;**53**(3/4):115-127

[26] Klinger BA. Density of Seawater [Internet]. p. 4. Available from: http://mason.gmu.edu/~bklinger/seawater.pdf

[27] De Sousa RMD. Carbon Prices. Dynamic analysis of European and Californian markets [doctoral dissertation]. Maio: Universidade Nova de Lisboa; 2014